A DIAGNOSTIC STUDY OF OUTGOING LONGWAVE FLUX USING ESTIMATES FROM RAW TOVS RADIANCES

Rolando Rizzi

European Centre for Medium range Weather Forecasts, Reading, U.K.

Summary. Several days of global raw TOVS data are processed to evaluate the ability of different forecast models to describe, using sequences of short range forecasts, features contained in the measured data. Radiance simulations are based on model fields obtained from a short-range (24 to 48 hours) forecast so that spin-up effect are mostly avoided and the description of the dynamical fields is still accurate. The simulations involve cloud parameters, cloud fraction and cloud liquid water. Estimates of outgoing longwave flux obtained from the measured and from the simulated radiances, using the same statistical regression, are compared with each other and with the quantity computed by the forecast model.

1. Introduction

The importance of cloud processes has always been recognized in climate studies and in the development of General Circulation Models (GCM), much less in Numerical Weather Prediction (NWP) until the extension of useful forecast length and the diversification in the products range has given new impulse to the development of more accurate parametrizations of diabatic processes (Ritter, 1992). The main reasons behind the asserted relevance of clouds are the large modifications induced by clouds in the distribution of heating and cooling at the Earth's surface and within the atmosphere (Browning, 1994).

As soon as a new prognostic cloud scheme (Tiedtke, 1993) is used operationally, the ECMWF model will acquire some capability to assimilate cloud-related information. Prior to this stage information contained in calibrated and earth located, or raw, TOVS (Tiros-N Operational Vertical Sounder) radiances is being used as a diagnostic tool to evaluate the ability of different models to describe, using sequences of short range forecasts, features contained in the measured data. The present exercise is therefore quite different from the diagnostics which employ long term integrations of the model to test its average properties against some independent data set.

The main difference between the raw TOVS radiances used in the present exercise and the radiances used operationally at ECMWF (Eyre at al. 1993) is the cloud clearing process which identifies and eliminates the data affected by clouds. Other differences are also present which will be discussed in section 2. Since the signature due to clouds on upwelling atmospheric radiance is quite outstanding at visible and infrared wavelengths, inadequacies in current schemes in representing cloud cover and cloud liquid water translate into large discrepancies. They allow therefore a detailed examination of aspects of the hydrological cycle and energetics which need to be improved in current NWP models as well as in GCMs.

Although the importance of clouds in NWP is perceived to lie in their radiative interactions, it is common practice to compare model cloud properties, such as cloud amount (either total or for thick layers) for example, with "equivalent" quantities belonging to data sets as independent as possible from the model, which nowadays are frequently derived from satellite radiance data (Rossow and Schiffer, 1985; Hamill et al. 1992; Stowe et al. 1991). It is possible that in such a comparison the same name (for example total cloud amount) is given to quite distinct quantities, obtained using different underlying assumptions (Morcrette, 1991a). Extreme care needs to be taken when comparing these satellite products among themselves and with model products (Hou et al. 1993). On the other hand once simulated radiances, obtained using all pertinent model information, are compared to measurements, one needs to be aware of the assumptions used in the simulations themselves. The evaluation of the errors is in both cases a delicate procedure, but certainly the retrieval step, total cloud cover in our example, makes the error estimation process particularly difficult and somewhat removed from the end user of the retrieved quantities.

In the present paper measured and simulated radiances are converted to longwave fluxes at the top of atmosphere (OLR) and compared. Details about the processing of TOVS radiances and the derivation of OLR are contained in section 2. Sections 3 and 4 discuss the characteristics of the short range forecasts used to simulate the radiances in presence of clouds.

2. Preprocessing of TOVS data.

Two data sets have been processed:

- level 1-B HIRS/2 (High Resolution Infrared Radiation Sounder/2) and MSU (Microwave Sounding Unit) data from 12UT 8 February to 06UT 11 February, 1989;
- TIP (Tiros Information Processor) data for 00UT 14 October to 06UT 16 October 1993.

Fourteen whole orbits around the Earth have been processed on average every day. In October 1989 the operational satellites were NOAA-10 and NOAA-11, while in October 1993 they were NOAA-11 and NOAA-12. The statistical results for the two dataset need to be evaluated separately because of the difference in platforms and instruments, as well as in the forecast models that have been used for the radiance simulations. The equatorial crossing time (ECT) for the ascending (A) and descending (D) orbit portion for the three platforms is significantly different. Each instrument therefore senses the atmosphere and the surface at different local time of the day. The ECT itself varies slowly during each platform's lifetime because the spacecraft does not make an integral number of revolutions per day and also because the orbit decays due to atmospheric drag and the satellite has to speed up, enhancing the effect. As a result the ECT (local time) for each platform and data set is:

- NOAA-10: February 89: 19:35 (A) and 7:35 (D);
- NOAA-11: February 89: 13:43 (A) and 1:43 (D);

October 93 : 16:11 (A) and 4:11 (D);

- NOAA-12: October 93 : 19:30 (A) and 7:30 (D).

Note the difference between NOAA-11 ECT in 1989 and 1993.

The ITPP (International TOVS Processing Package) has been used to process the data and to produce calibrated and earth located radiances. During preprocessing two brightness temperature datasets were generated, with and without a number of 'corrections' which are usually applied during the operational satellite data processing performed by NOAA-NESDIS (National Oceanic and Atmospheric Administration - National Environmental Satellite, Data and Information Service). These corrections consist of limb correction of HIRS/2 and MSU data, correction of HIRS/2 window channels for water vapour attenuation, correction for surface reflectivity and liquid water attenuation for MSU channels.

A secondary product of the processing is Outgoing Longwave Radiative flux (OLR) computed using a regression with HIRS/2 channels 1 to 12 corrected, as described above, as predictors. This OLR estimate is referred to as OLRTOV in the rest of the paper. The regression is part of the ITPP but is practically undocumented. It is however analogous to the technique described in Smith and Woolf (1983) used to obtain longwave radiation flux from VAS channels (VISSR Atmospheric Sounder), where it is found that the regression explains 99.9% of the simulated OLR variance in the clear case with a standard error of 1.2 Wm^{-2}, and 99.8% with a standard error of 2.2 Wm^{-2} in the cloudy case. Because of the close similarity between VAS and HIRS/2 spectral channels used in the regression, it is likely that the error estimates found in the referenced paper are applicable to the regression part of ITPP for clear and cloudy situations separately. In the ITPP however only one set of coefficients is used for any atmospheric condition, clear or cloudy.

Ellingson et al.(1989) have developed a similar technique to estimate OLR from HIRS/2 observations. Their regression analysis shows that 4 HIRS/2 channels are sufficient to explain 99.8% of the variance of the complete set of 3200 conditions with a root mean square error of about 2 Wm^{-2}. A validation of the technique is presented in Ellingson et al.(1990) by comparing nighttime homogeneous NOAA-9 ERBE scanner derived OLRs to estimates based on collocated HIRS measurements. They find that their HIRS technique yields flux data which tend to be lower by about 1-3 Wm^{-2} with rms differences of the order of 4 Wm^{-2} in all conditions except overcast conditions. In the latter case the HIRS estimates show a positive bias of 4 to 7 Wm^{-2} with rms differences in the range 6 to 10 Wm^{-2}. The authors conclude that the HIRS estimates agree with ERBE scanner observations as well as different ERBE scanners agree with each other.

In view of these results one can expect the ITPP regression to provide an estimate with an rms error of less than 10 Wm^{-2}, including in the error budget the errors introduced by the

brightness temperature corrections discussed above. Not much is known on systematic errors introduced by the ITPP regression. Since the same technique is applied to simulated and measured radiances (to produce respectively OLRTOV and OLRSIM), relative biases can be produced when the regression is applied to very different atmospheric situations, such as radiance measurements in a cloudfree area, while simulated radiances contain a significant amount of clouds. In these conditions however the bias is much smaller than the difference in the two estimates.

The spacing between HIRS/2 scanning lines is about 42 km and the spacing between Field of Views (FOVs) ranges from about 26 km at the centre of the scan to about 81 for the outer FOVs. The resolution of a field of HIRS/2 measurements can be defined as their mean spacing and is therefore about 40 Km. There is also a spatial averaging involved since FOV equivalent circular diameter ranges from about 17.4 km (FOV area of 235 km^2) to about 40km (1260 km^2). The resolution of HIRS/2 measurements is therefore higher than the model resolution which can be estimated to be about 80 km. To reduce the effect of sub-grid scale processes present in the measurements, each orbit radiance field and the OLR field has been filtered using a bi-dimensional gaussian filtering function (Amato et al., 1991) to reduce the resolution to about 90 km. In the following text any reference to measured radiances relates to filtered radiances unless otherwise specifically stated.

3. Forecast runs and spin-up effect

Radiance simulations are based on model fields obtained from a short-range forecast so that the description of the dynamical fields is most accurate. In order to define the shortest forecast length, in view of the operational model spin-up time, a comparison was made among OLR computed by operational forecasts of various lengths for midnight of every day in the period from October 1, 1992 to end of Febrary 1993. It is found that the OLR field decreases slightly with increasing forecast length, an effect probably caused by some increase in mean cloudiness as convection becomes stronger. However the differences in OLR between the different forecasts tend to grow rapidly in root mean square sense, an effect probably caused by growing discrepancies in the circulation patterns generated by the forecasts. In view of these results satellite data has been compared with simulations produced using the second day of the forecast for each day of data. It has been assumed that the spin-up time of the various versions of the forecast model used in the present paper is not longer than that of the operational model.

A number of forecast experiments were run, all at resolution T213 and with 31 vertical levels, involving 4 different versions of the forecast model:

- 1989 data:
    1. New Cloud Scheme (NCS) within the operational spectral model (SPM) cycle 46 (NCS46);
    2. SPM cycle 46 (SPM46) used as control experiment ;

- 1993 data:
    1. NCS within the operational spectral model (SPM) cycle 48 (NCS48);
    2. SPM cycle 48 (SPM48) used as control experiment.

In all cases the forecasts were started from initialized analyses produced by the assimilation system which was operational at the time the satellite data were measured.

A complete description of the differences among the various experiments is beyond the scope of the present paper. Model changes between cycle 46 and 48 of the SPM involve the boundary layer and the land surface parametrizations (Betts et al. 1993). The parametrization of air-sea interaction has also been modified (Miller et al. 1992). A brief account of the salient differences between the experiments is given below with the aim of increasing the understanding of the differences found between simulated and measured data.

Clouds in SPM (both cycle 46 and 48) are determined diagnostically (Slingo, 1987). The cloud cover of stratiform clouds is diagnosed from the large scale values of relative humidity, vertical velocity and the temperature lapse rate across boundary layer inversions. Convective cloudiness is diagnosed from the precipitation rate produced by the model convection scheme. Cloud water content is prescribed as the equivalent of a supersaturation of 5% for stratiform clouds and a fixed mixing ratio of 0.1 g/kg for convective clouds.

The NCS applied to both cycles 46 and 48 is described in Tiedtke (1993). It is a prognostic approach where the time evolution of the cloud variables, cloud cover and cloud water content, is determined by the sources and sinks due to the various cloud processes, i.e. clouds form as the result of adiabatic and diabatic cooling, cumulus convection and boundary layer turbulence and clouds dissipate through adiabatic and diabatic heating, turbulent mixing of cloud air with unsaturated environmental air and precipitation processes. An important feature of this scheme is the explicit representation of anvil and cirrus clouds in connection with penetrative cumulus convection. Their time evolution is determined by the horizontal advection of condensate from convective updrafts into environmental air as well as by precipitation processes, large scale lifting and radiative transfer. The treatment of the precipitation process for ice, which plays a dominant role for the maintenance of the ice content, is based on Heymsfield and Donner (1990) in that the loss of cloud ice is determined by sedimentation of ice crystals where fallspeeds are used in agreement with observational data.

In Cycle 48 of SPM a skin layer has been introduced over land with no heat capacity so that its temperature adjusts instantaneously to the radiative forcing. Some decoupling is obtained between surface and lower atmosphere so that the surface temperature is allowed to increase during daytime without increase of 2-metre temperature and soil heat flux. In cycle 46 the upper surface layer is a 7.2 cm deep homogeneous layer and the surface temperature is the

average soil temperature of the upper layer.

4. Radiance simulation in presence of clouds

Radiances for a clear atmosphere are computed using surface skin temperature and the temperature and humidity profiles. The simulation of cloud effects requires additional input fields, namely Cloud Fraction (CF) and Cloud Liquid Water (CLW). All model fields are initially interpolated spatially and temporally to each measurement FOV. Cloud emissivity is then computed from (interpolated) CLW using an algorithm similar to the one used in the ECMWF operational radiation scheme (Morcrette, 1991b) but applied to a directional radiance instead of a flux and incorporating the computation of layer integrated liquid water path and corrections for multiple scattering and ice/water percentage. The effective liquid water absorption coefficient is assumed independent of frequency. The layer effective cloud fraction (ECF - fraction of FOV covered by a cloud whose emissivity is unity) is then computed as the product of emissivity times CF. The vertical profile of ECF as seen from the top of the atmosphere (PECF) is required to compute the radiance emerging from the model FOV; PECF is computed using either a random overlap assumption or a maximum overlap in a way similar to the treatment in the model radiation scheme. The summation over all model layers of PECF represents the fraction of FOV which is covered by clouds. The forward radiance model RTTOV (Eyre, 1991) is used to compute the clear radiances in all HIRS/2 and MSU channels and the set of overcast radiances (ORS) that would be observed, in every measurement channel, if a black cloud covering the entire FOV were present at any one of the 40 pressure layers into which the atmosphere is divided for radiance computation purposes. The top temperature of the cloudy layer is assumed equal to the model temperature interpolated to the top of the layer. Since the ORS are slowly varying functions of height, a simple linear interpolation scheme is used to compute overcast radiances at model levels (ORM). The knowledge of PECF and ORM allows us to compute the simulated cloudy radiance:

$$R(j) = \sum_{1}^{N} PECF(l) \cdot ORM(j,l) + SF \cdot ORM(j,0)$$

where N is the number of model layers, j is the spectral channel being simulated, and ORM(j,0) is the radiance emitted by the underlying surface. No bias or scan correction is applied to simulated radiances.

The same linear regression described in section 2 is used to compute the simulated OLR (OLRSIM) from simulated radiances in HIRS/2 channels 1 to 12.

5. Results.

As explained in sections 2 and 4, three estimates of outgoing longwave flux at the top of atmosphere (OLR) are produced: OLR derived from HIRS/2 radiance measurements

(OLRTOV), OLR derived from simulated HIRS/2 radiances (OLRSIM) and instantaneous OLR generated by the forecast model (OLRMOD). Deriving an estimate of OLR from the measurements and the simulations is about the only way to compare the model radiative flux scheme with the radiation scheme used for the present simulations. In the following, results are shown for a comparison involving the three OLR estimates. No effects linked to the daily cycle have yet been systematically investigated, the latter requiring separate processing of the ascending and descending orbit portions for each satellite.

5.1 *The 1989 dataset.*

Tables 1 and 2 show the mean (BIAS) and standard deviation (STDEV) of the differences between the three OLR estimates using respectively unfiltered and filtered raw radiances. The operational forecast SPM46 is used for both datasets and hence the two tables differ only in the resolution of the NOAA-11 data. The global bias is reduced by 1% and the standard deviation by 10% when comparing simulated and model values against satellite derived OLRs. Very nearly identical results are obtained for NOAA-10, NCS forecasts and for the 1993 dataset. Since filtering of the measured radiances is based on sound principles and reduces the standard deviation, only results with filtered data will be presented hereafter.

Table 3 shows results for NCS46. Comparing them to SMP46 results (Table 2) the reduction in global bias between OLRSIM and OLRTOV is significant but is not accompanied by a reduction in standard deviation. For NOAA-11 data, both models produce differences over land usually smaller in both bias and standard deviations than those over sea.

Tables 4 and 5 contain zonally averaged bias and standard deviation for SPM46 and NCS46. Each zonal band extends 20 degrees in latitude and is centred at the value shown in the tables. The bias is seen to possess a large zonal variability and largest values of standard deviation are found at latitudes from 30 South to 10 North. The OLRSIM bias reduction going from SPM46 to NCS46 is apparent at all latitudes except over sea in the Arctic region.

Figs. 1a and 1b are bidimensional histograms of OLRTOV (abscissa) against OLRSIM for the whole 1989 dataset. OLRSIM is computed with SPM46 (1a) and NCS46 (1b). The shaded portions are areas of constant density (logarithm of number of points within a 2-dimensional bin normalized to the total number of points). From the discussion on the error in the computation of OLRTOV, in section 2, it follows that the error in the computation of OLRSIM is expected to dominate.

Several points are worth noting:

a. a large portion of the data lies along the diagonal;
b. there is a clear underestimation of the magnitude of the largest OLR values in both models;
c. the scatter plot for NCS46 is more symmetrical around the diagonal than the SPM46

TABLE 1

Global bias and standard deviation of the differences between OLRSIM, OLRMOD and OLRTOV (Wm^{-2}). Unfiltered HIRS/2 data. Model: SPM46. 1989 dataset.

NOAA-11	NTOT	OLRSIM-OLRTOV		OLRMOD-OLRTOV		OLRMOD-OLRSIM	
		BIAS	STDEV	BIAS	STDEV	BIAS	STDEV
GLOBAL	1895339	15.1	33.7	11.0	34.3	-4.1	18.6
LAND	668984	9.2	29.3	11.0	30.3	1.9	16.8
SEA	1226355	18.3	35.2	10.9	36.0	-7.3	18.6

TABLE 2

Global bias and standard deviation of the differences between OLRSIM, OLRMOD and OLRTOV (Wm^{-2}). Filtered HIRS/2 data. Model: SPM46. 1989 dataset.

NOAA-11	NTOT	OLRSIM-OLRTOV		OLRMOD-OLRTOV		OLRMOD-OLRSIM	
		BIAS	STDEV	BIAS	STDEV	BIAS	STDEV
GLOBAL	1898598	14.9	30.4	10.8	31.2	-4.1	18.6
LAND	672230	8.7	26.4	10.5	27.7	1.8	16.8
SEA	1226368	18.3	31.7	11.0	32.6	-7.3	18.6
NOAA-10	NTOT	OLRSIM-OLRTOV		OLRMOD-OLRTOV		OLRMOD-OLRSIM	
		BIAS	STDEV	BIAS	STDEV	BIAS	STDEV
GLOBAL	1968397	9.2	29.0	11.7	30.5	2.5	18.4
LAND	703211	8.4	23.3	16.1	24.2	7.6	15.5
SEA	1265186	9.6	31.4	9.3	33.1	-.3	19.2

TABLE 3

Global bias and standard deviation of the differences between OLRSIM, OLRMOD and OLRTOV (Wm^{-2}). Model: NCS46. 1989 dataset.

NOAA-11	NTOT	OLRSIM-OLRTOV		OLRMOD-OLRTOV		OLRMOD-OLRSIM	
		BIAS	STDEV	BIAS	STDEV	BIAS	STDEV
GLOBAL	1898598	8.2	31.0	8.8	32.8	.7	20.4
LAND	672230	2.7	27.9	8.9	28.2	6.2	18.4
SEA	1226368	11.2	31.7	8.8	34.8	-2.4	20.6
NOAA-10	NTOT	OLRSIM-OLRTOV		OLRMOD-OLRTOV		OLRMOD-OLRSIM	
GLOBAL	1968397	3.4	29.0	9.2	32.1	5.8	19.4
LAND	703211	3.9	23.7	13.3	24.4	9.5	16.2
SEA	1265186	3.1	31.3	6.9	35.2	3.8	20.5

TABLE 4

Zonal bias and standard deviation of the differences between OLRSIM and OLRTOV (Wm^{-2}). Data for NOAA-11 and NOAA-10. 1989 dataset.

ZONAL ALL DATA		SPM46		NCS46	
LAT	NTOT	OLRSIM-OLRTOV		OLRSIM-OLRTOV	
		BIAS	STDEV	BIAS	STDEV
-80.0	362453	8.2	16.7	5.7	16.3
-60.0	460681	14.0	26.1	6.3	25.5
-40.0	432461	8.5	30.2	4.0	30.3
-20.0	422527	15.0	40.1	7.1	38.8
.0	434233	19.1	37.5	13.1	40.3
20.0	438605	6.4	28.2	.3	29.0
40.0	444302	10.4	27.0	-.2	26.4
60.0	477014	11.3	21.3	4.5	20.8
80.0	394719	14.5	17.2	11.8	17.2

TABLE 5

Zonal bias and standard deviation of the differences between OLRSIM and OLRTOV (Wm^{-2}). Data for NOAA-11 and NOAA-10. 1989 dataset.

	ZONAL OVER LAND					ZONAL OVER SEA				
LAT	NTOT	-- SPM46--		-- NCS46--		NTOT	-- SPM46--		-- NCS46--	
		BIAS	STDEV	BIAS	STDEV		BIAS	STDEV	BIAS	STDEV
-80.0	271757	6.4	14.6	3.1	13.5	90696	13.5	20.3	13.8	19.8
-60.0	32252	10.4	16.1	9.3	15.6	428429	14.3	26.6	6.0	26.0
-40.0	34809	-.8	22.4	-4.7	23.8	397652	9.3	30.2	4.7	30.2
-20.0	93925	20.8	42.3	7.4	43.8	328602	13.3	37.9	7.0	35.5
.0	108575	27.4	39.5	16.6	42.6	325658	16.5	35.8	12.0	38.5
20.0	154201	1.4	19.8	-4.2	22.1	284404	9.2	29.7	2.7	29.5
40.0	220627	4.1	19.8	-1.6	19.9	223675	16.7	30.9	1.2	30.0
60.0	323185	7.7	17.3	4.7	17.7	153829	19.0	26.1	4.1	25.8
80.0	136110	9.1	15.2	3.7	15.3	258609	17.3	17.0	16.0	16.6

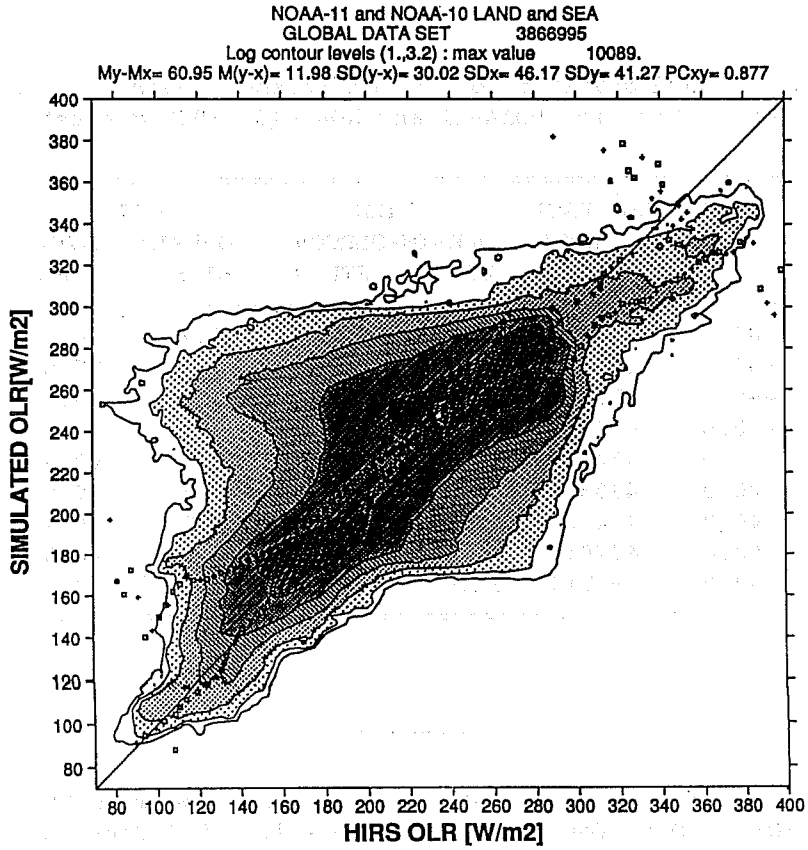

Fig. 1a. Bi-dimensional histogram of outgoing longwave flux at the top of atmosphere (OLR) computed from measured HIRS/2 radiances (ORTOV) versus simulated OLR (OLRSIM) computed using the forecast model SPM46. Period: from 12GMT 8 Feb. 1989 to 06GMT 11 Feb. 1989.

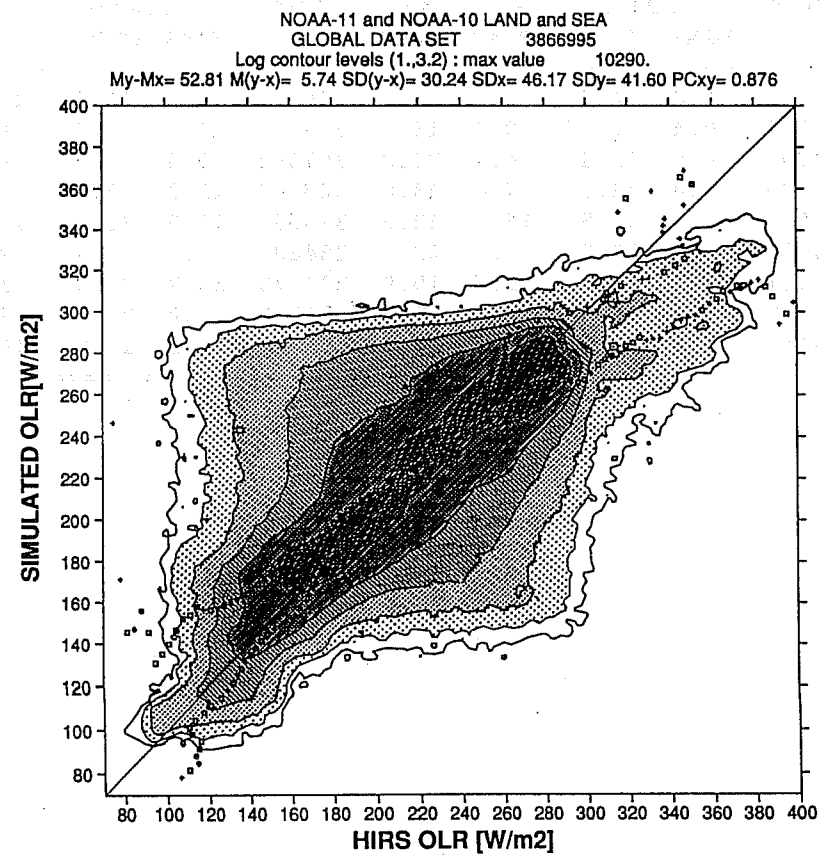

Fig. 1b. As in Fig. 1a. but OLRSIM is computed using forecast model NCS46.

one, which explains the smaller overall bias at the expense of a larger standard deviation.

d. the fit of NCS46 to the data in the area of lowest OLR values is worse than SPM46.

Figs. 2a and 2b show the scatter plots for NCS46 for land and sea points separately. The problem pointed out in b. is clearly due to underestimation of the longwave fluxes emerging from land. In fact the largest differences are found for the afternoon hours (NOAA-11) over clear areas; differences of 40 Wm^{-2} can often be found over large areas of the Sahara Desert (at 12 UT), the clear portions of South America (18 UT), Australia and India (06 UT). The time evolution of the observed differences in brightness temperature (using measured and simulated values for channel 8 of HIRS/2) over these areas in clear sky conditions shows that the simulated values are too low by as much as 10-15K over the desert areas in the warmest hours of the day, sensed by NOAA-11, and the reduction in brightness temperature in the afternoon is slower that the one observed, indicating a phase error as well. Similar findings are also reported in Morcrette, 1991a, where simulated brightness temperatures for the longwave channel of Meteosat are compared to reduced resolution measured data. There are several physical mechanisms that could explain the observed discrepancy: an underestimation of the skin temperature by the model's surface scheme, while the radiance simulation could introduce errors due to inaccurate water vapour absorption (for both continuum and lines) and the absence of any aerosol effects. However the latter forward simulation deficiencies cannot explain the large observed differences over the deserts, where the amount of integrated water vapour in the atmosphere is very low, and over large areas. The likely explanation is that the average temperature for the first layer is not representative of the temperature of the first few millimetres of soil. In fact the results obtained with the 1993 dataset, discussed later, show the large effects on skin temperature that have been achieved by the change in the description of the surface physics in cycle 48 of the forecast model.

The underestimation under discussion is the cause for some of the large variability noticed in zonal bias for both models . In latitude belts where large continental areas are found with low mean cloudiness, at this time of the year, the underestimation caused by a colder earth surface, in areas free of clouds, counteracts the general overestimation caused by insufficient cloud development giving rise to low bias values; in areas where cloudiness is more widespread, like the ITCZ, the bias is generally large and positive.

Regarding the point c. noted above, the relatively larger asymmetry of the scatter in the mid portion of the plot for SMP46, when compared to NCS46, is due to OLRTOV reaching values as low as 120 Wm^{-2} while lowest values from SPM46 are about 160 Wm^{-2}. A similar problem is reported by Morcrette (1991a). These large differences are attributable both to inaccurate physics and circulation patterns. A symmetric (however spread) scatter is in fact a necessary, but not sufficient, condition to consider the physical parametrizations as adequate, the scatter being then due mostly to positional errors in the circulation pattern. By physical

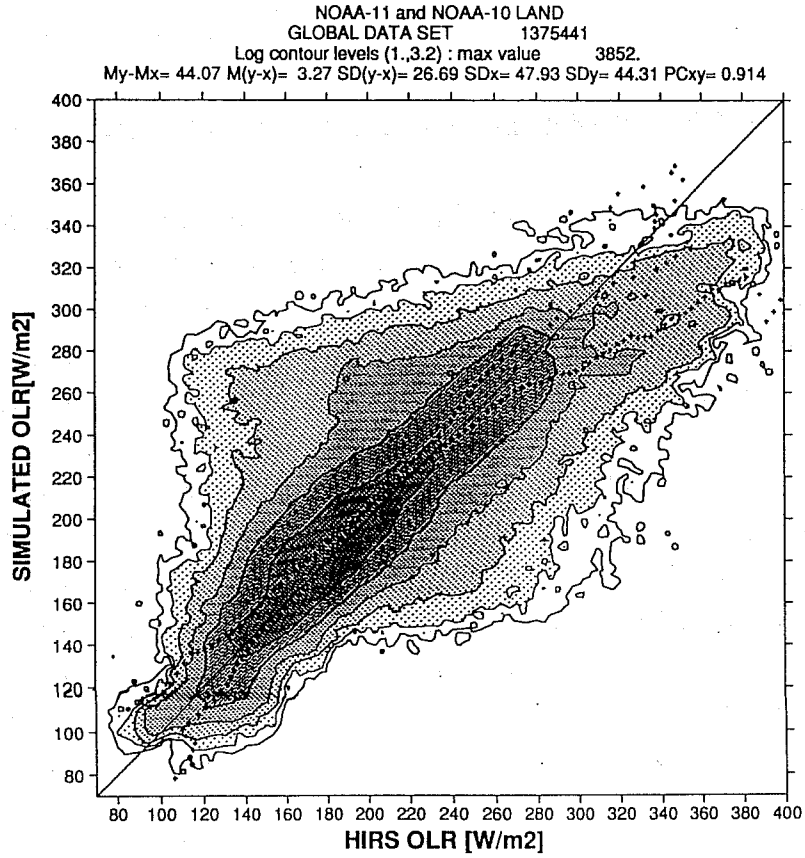

Fig. 2a. As in Fig 1b. for all FOVs over land.

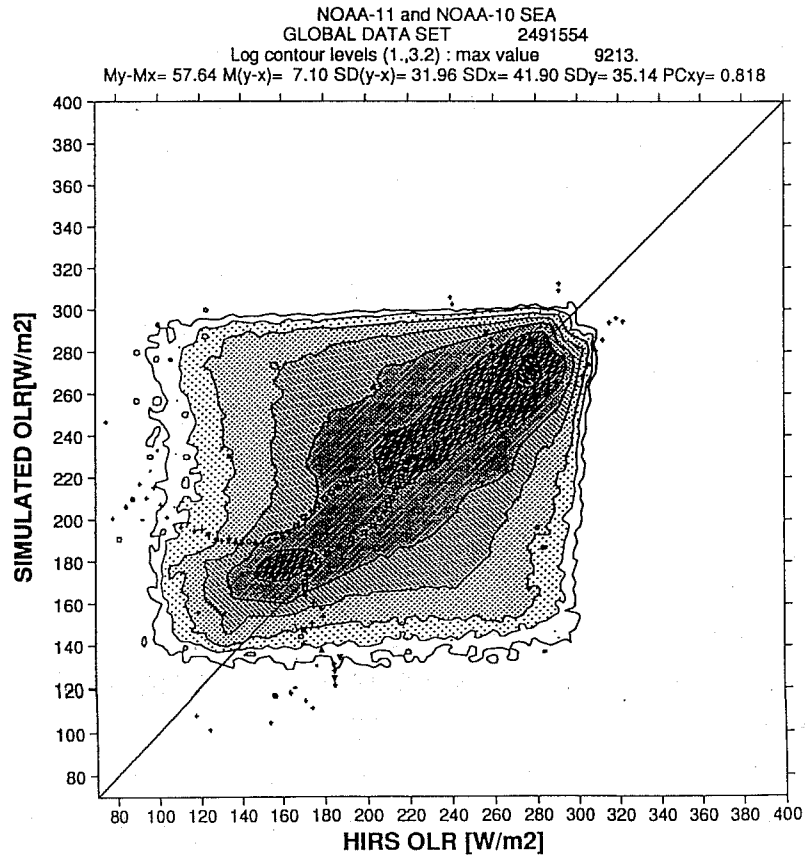

Fig. 2b. As in Fig 1b. for all FOVs over sea.

parametrization here it is meant those processes which have some impact on the radiance fields, and the derived OLR. Although the radiative characteristics of clouds and of the earth's surface in the infrared are of great relevance, HIRS/2 radiances contain information on water vapour, integrated over relatively thick layers, and this information is implicitly included in the OLR estimates. The overall results for the NCS46 model show an improvement in the description of the radiative properties of the atmosphere over sea and, to a lesser extent, over land. After examining individual six-hourly scatter plots (not shown) it is found that most of the asymmetry for SPM46 originates from data in the latitude belt from 30 to 10 degrees south, where the ITCZ is found at this time of the year.

The results described in point d., namely the large warm OLR bias in the Arctic and in the Antarctic region over sea, can be further examined using the simulated radiances in the window channel (channel 8 of HIRS/2). These show an overall warm bias of 6.1 K over the Arctic seas. There may be several causes for the observed discrepancy: no forward model bias correction scheme is applied in absence of clouds; there may be differences in the structure of model clouds with respect to the real arctic clouds, and the model surface temperature, in the presence of extremely cold sea ice, may be different from the actual temperature. The bidimensional histogram of the differences in OLR and channel 8 brightness temperatures for the latitude band from 80 to 90 North, shown in fig. 3a and 3b, indicate that the core of the simulated values is offset, while some spread is probably caused by clouds, which indicates that the model values for ice surface temperature are the main reason for the observed warm bias, a results reported also in Morcrette (1991a). Nearly the same problem is found over sea in the latitude region from 70 to 90 South.

The images of Figures 4 to 6 show the geographical distribution respectively of OLRTOV (fig. 4), OLRSIM obtained from SPM46 (fig. 5) and NCS46 (fig. 6), for a six hour period centered at 12UT of 8 February 1989. All the images use the same colour code. The measured data clearly show the Sahara region and its large OLR flux (up to 370 Wm^{-2}) and the location of the ITCZ in the Indian and Pacific oceans slightly south of the Equator.

The tabulated data, the histograms and the geographical distribution of the OLR fields clearly indicate that while SPM46 provides a fair description of the area extent of the organized convection, it severely underestimates its depth, OLRTOV being much colder than simulations; differences of 60-100Wm^{-2} are found in any deep convection area over the oceans and over land both in the tropical region and at mid-latitudes. Experiment NCS46 shows a very different OLR distribution. The description of mid-latitude systems is improved. Much lower values are found in convective areas, denoting a more vigorous cloud development, but they cover only a fraction of the real convective regions. There are in fact areas in experiment SPM46 which emit moderate OLR values appearing as if completely covered with low level cloudiness, capable of shielding the emission from the surface, while they are nearly free of clouds in NCS46.

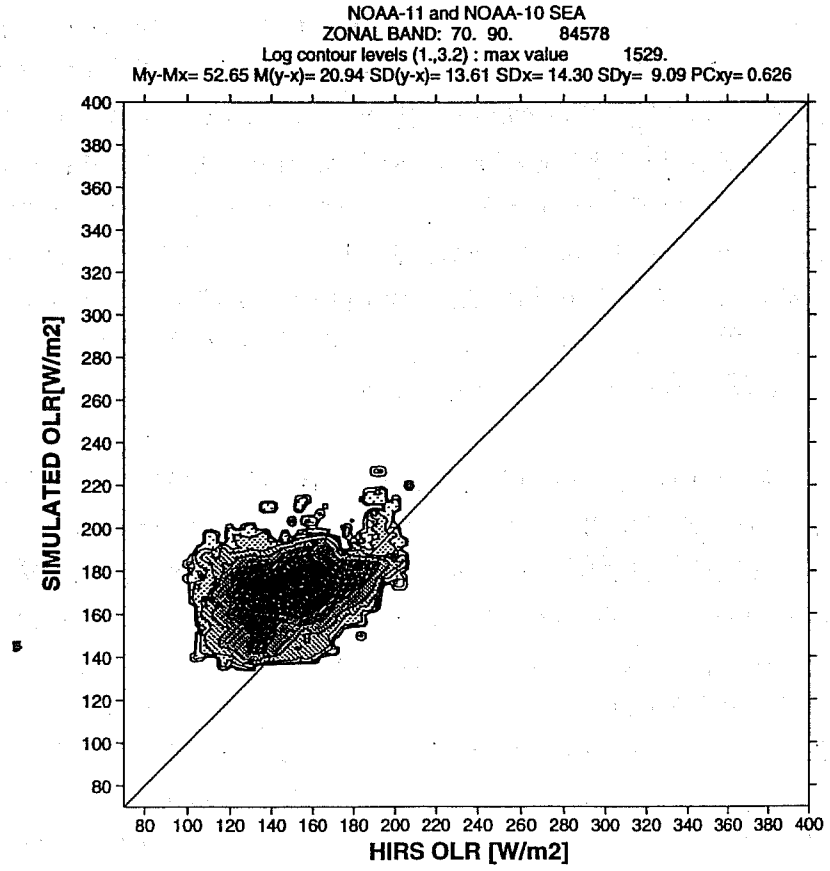

Fig. 3a. As in Fig 2b. for data in the latitude band from 70 to 90 North (over sea).

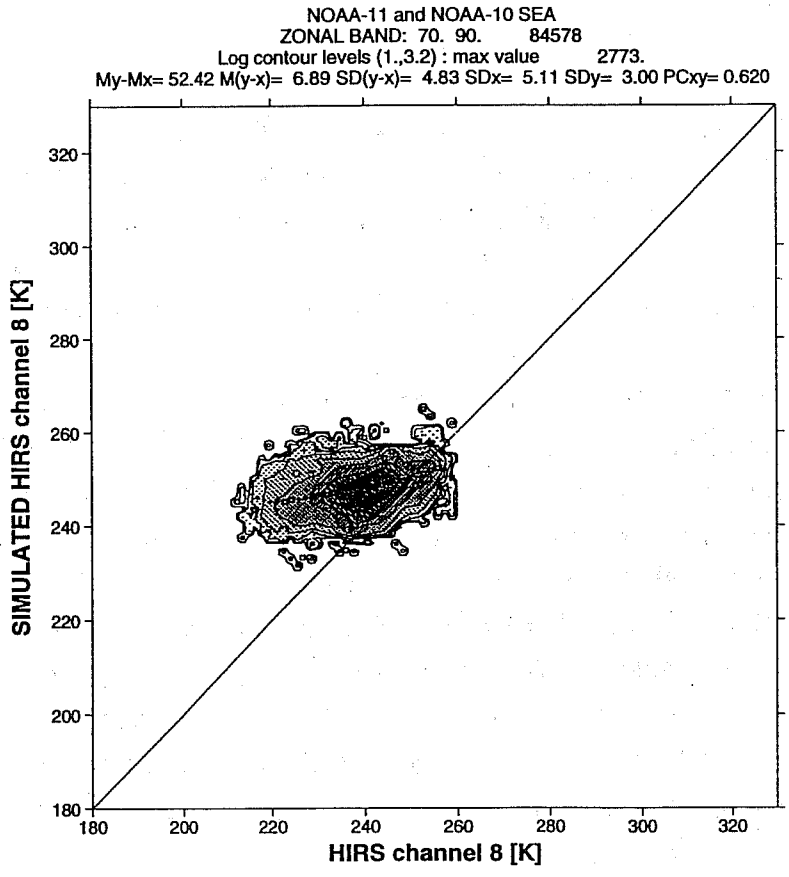

Fig. 3b. Bi-dimensional histogram of brightness temperature in HIRS/2 channel 8 versus the simulated value using forecast model NCS46. Data in the latitude band from 70 to 90 North over sea. Period: from 12GMT 8 Feb. 1989 to 06GMT 11 Feb. 1989.

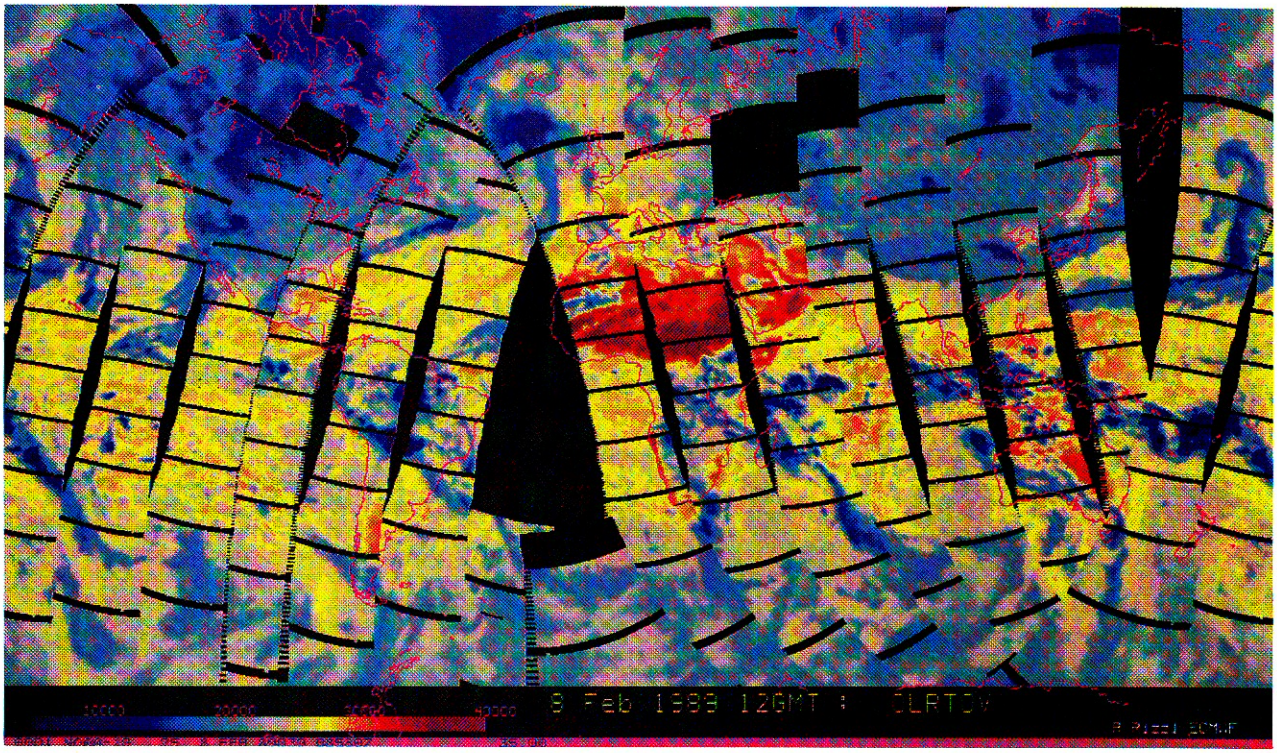

Fig. 4. OLR obtained from HIRS/2 measurements (OLRTOV) for a six-hour period centered at 12GMT, 8 Feb. 1989. The data is displayed in Mercator projection and is color coded in the range 60 (navy blue) to 400 (purple) Wm^{-2}. Black points indicate locations where data is missing (calibration cycle, data parity error or data outside the six-hour window).

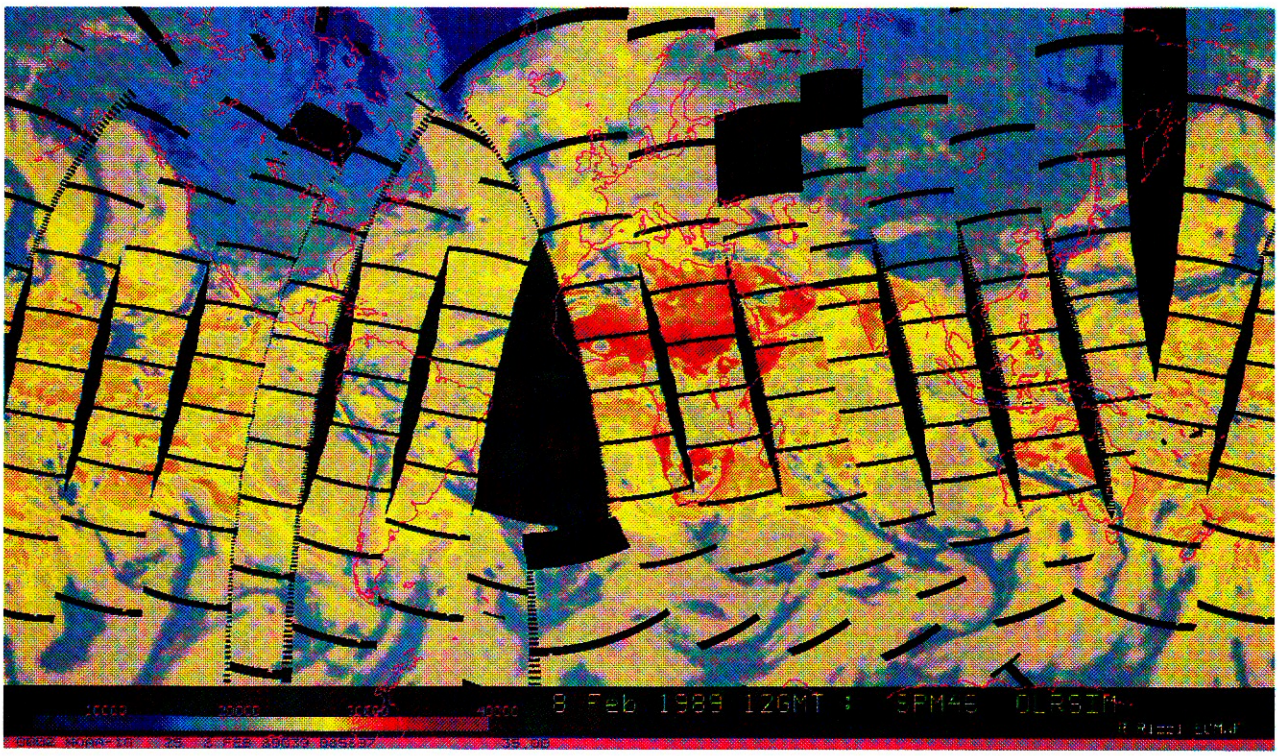

Fig. 5. Same as in Fig. 4 but simulated OLR (OLRSIM) computed using SPM46 is shown.

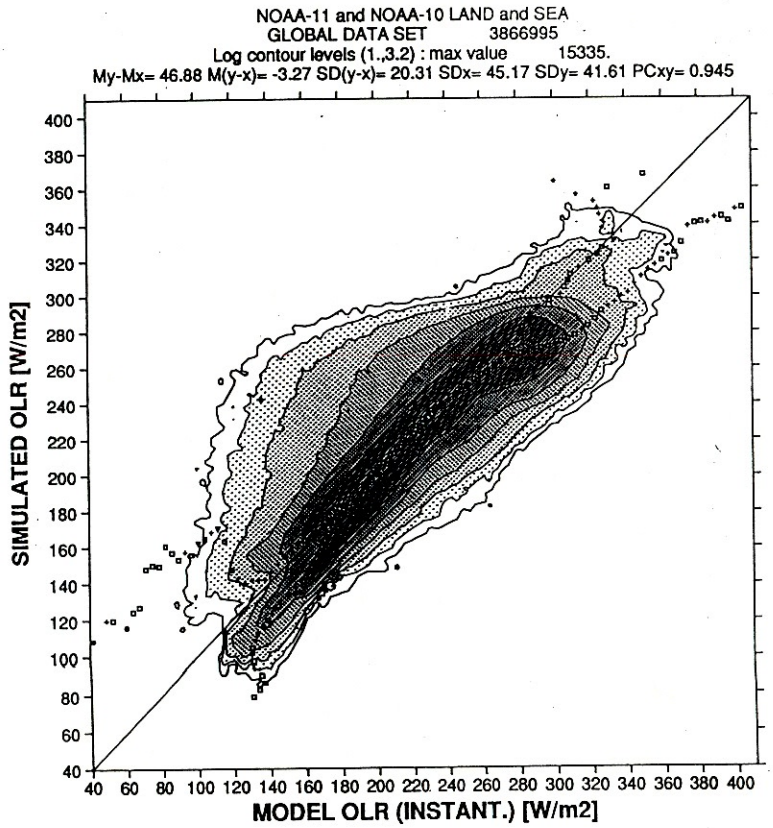

Fig. 7. Bi-dimensional histogram of OLR directly computed during the NCS46 run (OLRMOD on the abscissa) and using the simulated radiances (OLRSIM on the ordinate) using the same model NCS46. Global data set for the period from 12 GMT 8 Feb. 1989 to 06GMT 11 Feb. 1989.

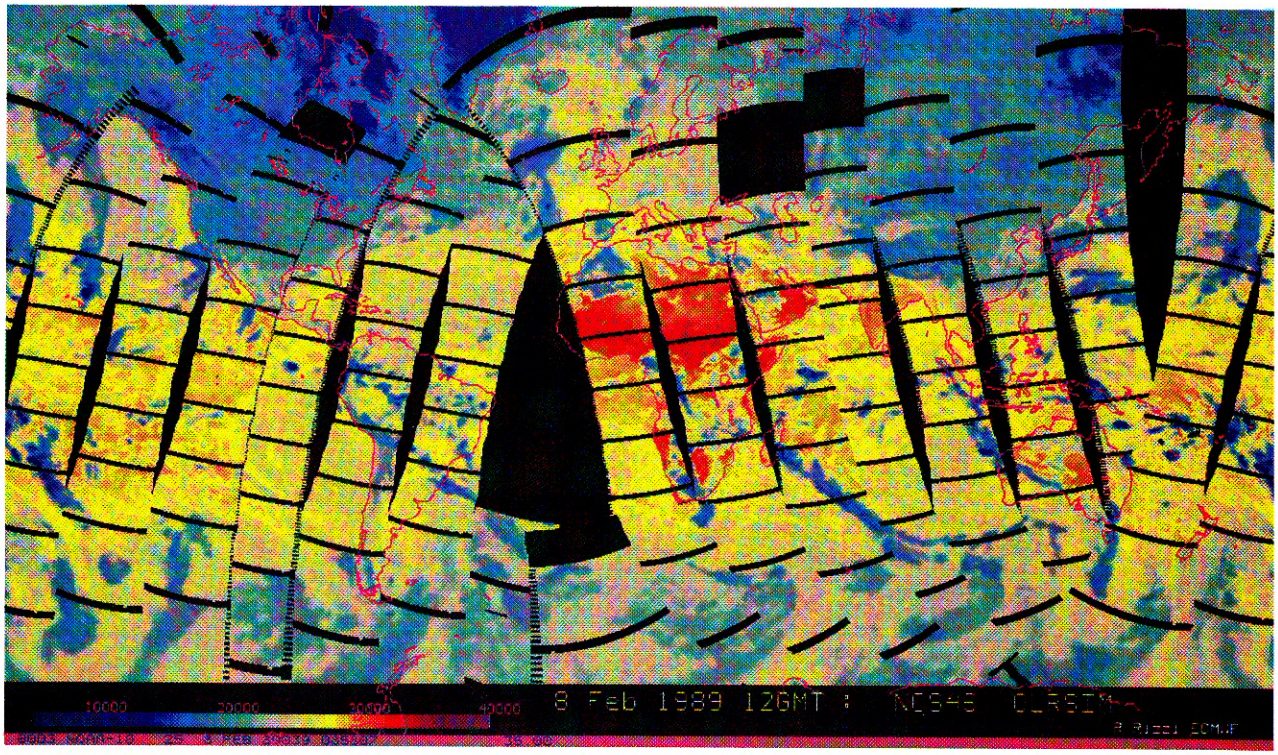

Fig. 6. Same as in Fig. 4 but simulated OLR (OLRSIM) computed using NCS46 is shown.

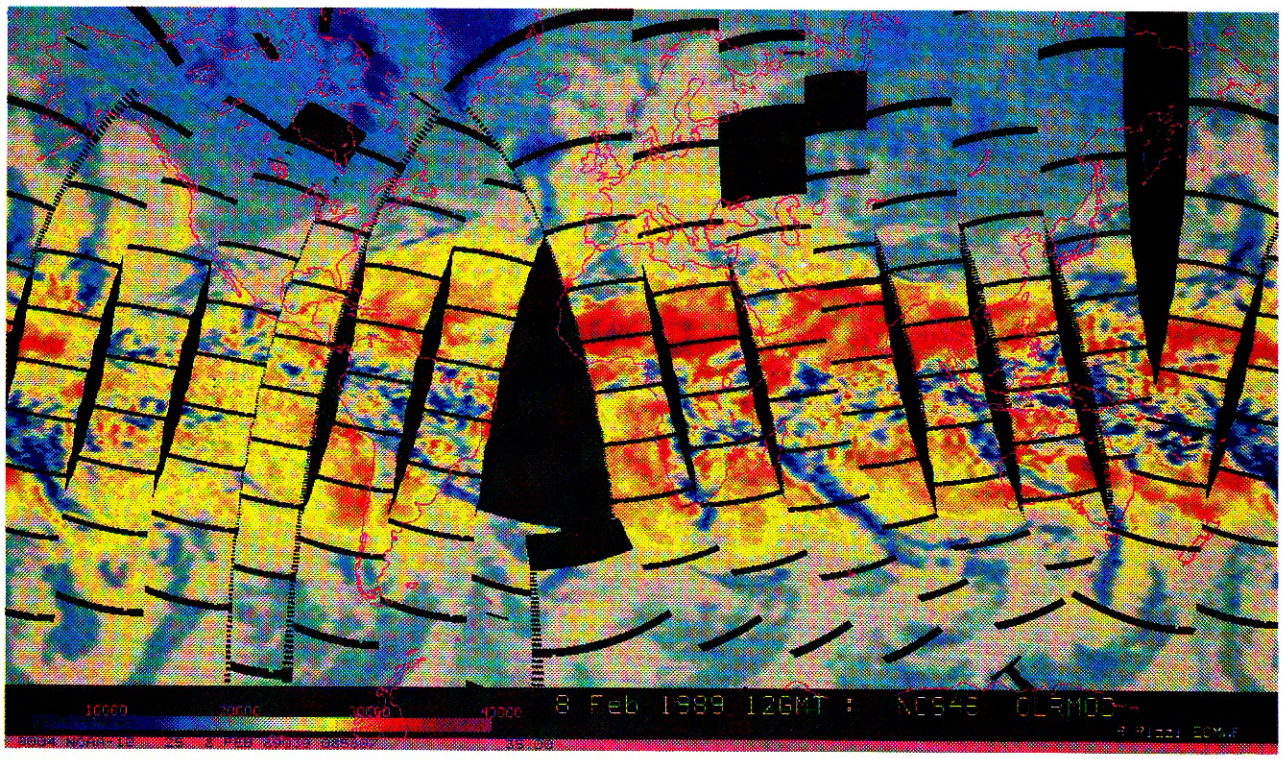

Fig. 8. Same as in Fig. 4 but OLR computed by the forecast (OLRMOD) model NCS46 is shown.

TABLE 6

Zonal bias and standard deviation of the differences between OLRMOD and OLRTOV (Wm^{-2}). Data for NOAA-11 and NOAA-10. 1989 dataset.

	ZONAL OVER LAND					ZONAL OVER SEA				
LAT	NTOT	-- SPM46--		-- NCS46--		NTOT	-- SPM46--		-- NCS46--	
		BIAS	STDEV	BIAS	STDEV		BIAS	STDEV	BIAS	STDEV
-80.0	271757	17.8	14.4	16.4	12.2	90696	6.7	22.1	11.0	19.8
-60.0	32252	5.5	16.3	9.0	15.4	428429	4.0	27.4	2.4	26.1
-40.0	34809	.5	26.6	1.2	25.5	397652	8.2	33.3	9.1	33.3
-20.0	93925	15.0	42.6	4.6	46.1	328602	13.3	38.2	9.4	40.9
.0	108575	23.0	39.9	13.5	45.0	325658	12.7	39.1	7.8	46.5
20.0	154201	14.8	26.3	14.1	25.8	284404	15.4	33.4	14.3	34.3
40.0	220627	11.0	20.6	9.2	20.5	223675	9.0	30.8	2.5	30.4
60.0	232185	7.5	18.5	7.7	18.3	153829	3.7	24.8	-4.0	26.1
80.0	136110	16.9	15.1	14.7	14.3	258609	15.8	18.0	16.5	18.3

TABLE 7

Zonal bias and standard deviation of the differences between OLRMOD and OLRSIM (Wm^{-2}). Data for NOAA-11 and NOAA-10. Model: NCS46. 1989 dataset.

	OVER LAND			OVER SEA		
LAT	NTOT	BIAS	STDEV	NTOT	BIAS	STDEV
-80.0	271757	13.3	8.2	90696	-2.8	5.9
-60.0	32252	-.4	9.5	428429	-3.7	9.1
-40.0	34809	5.9	16.7	397652	4.4	15.1
-20.0	93925	-2.8	26.8	328602	2.4	28.2
.0	108575	-3.1	25.0	325658	-4.2	28.7
20.0	154201	18.2	15.9	284404	11.7	21.5
40.0	220627	10.7	13.1	223675	1.2	14.8
60.0	323185	2.9	12.0	153829	-8.0	12.3
80.0	136110	11.0	10.9	258609	.4	11.1

TABLE 8

Global bias and standard deviation of the differences between OLRSIM, OLRMOD and OLRTOV (Wm^{-2}). Model: SPM48. 1993 dataset.

NOAA-11	NTOT	OLRSIM-OLRTOV		OLRMOD-OLRTOV		OLRMOD-OLRSIM	
		BIAS	STDEV	BIAS	STDEV	BIAS	STDEV
GLOBAL	1213986	14.4	30.9	11.8	30.8	-2.6	18.5
LAND	424608	8.5	29.1	11.1	27.4	2.5	17.7
SEA	789378	17.5	30.7	12.1	31.9	-5.4	18.2
NOAA-12	NTOT	OLRSIM-OLRTOV		OLRMOD-OLRTOV		OLRMOD-OLRSIM	
		BIAS	STDEV	BIAS	STDEV	BIAS	STDEV
GLOBAL	1325127	8.7	28.5	14.8	29.9	6.1	18.7
LAND	484966	4.2	27.8	13.7	27.6	9.5	16.4
SEA	840161	11.3	28.5	15.5	30.9	4.2	19.5

TABLE 9

Global bias and standard deviation of the differences between OLRSIM, OLRMOD and OLRTOV (Wm^{-2}). Model: NCS48. 1993 dataset.

NOAA-11	NTOT	OLRSIM-OLRTOV		OLRMOD-OLRTOV		OLRMOD-OLRSIM	
		BIAS	STDEV	BIAS	STDEV	BIAS	STDEV
GLOBAL	1213986	6.0	30.1	6.3	32.8	.4	19.9
LAND	424608	3.3	28.3	8.0	27.8	4.7	18.6
SEA	789378	7.4	30.3	5.5	34.5	-2.0	20.1
NOAA-12	NTOT	OLRSIM-OLRTOV		OLRMOD-OLRTOV		OLRMOD-OLRSIM	
		BIAS	STDEV	BIAS	STDEV	BIAS	STDEV
GLOBAL	1325127	1.8	28.2	9.6	32.3	7.9	19.9
LAND	484966	.1	27.5	11.2	28.2	11.1	17.3
SEA	840161	2.7	28.3	8.8	34.1	6.0	20.7

The discussion of the differences between OLRSIM and OLRTOV is applicable to a large extent also to the differences found when comparing OLRMOD versus OLRTOV. The OLRMOD values from NCS46 generally produce a better fit to the data than the values obtained from SPM46 in terms of bias albeit an increase in standard deviation as already noted when discussing the OLRSIM data. Zonal differences are shown in Table 6 for both models. The main fact to be added is the large warm biases seen in both the polar regions over land with NCS46, not present in the OLRSIM data.

To address further the differences between OLRMOD and OLRSIM, within the NCS46 model, Table 7 shows the zonal statistics, Fig. 7 the scatter plot of OLRMOD (abscissa) versus OLRSIM, and Fig. 8 the geographical distribution of OLRMOD at the same time as in Fig 4, 5 and 6. It is found that:

a. in the latitude band from 30N to 30S in cloudfree areas OLRMOD is clearly higher than OLRSIM (and OLRTOV) by up to 30 Wm^{-2};
b. convective areas as described by OLRMOD are clearly more widespread;
c. at mid latitudes, up to 65N and 65S, OLRMOD frontal regions are colder and their geographical extent is larger than in OLRSIM;
d. there is a fairly large positive OLRMOD bias over land in both polar regions (above 70 N or below 70 S).

These differences do not yet have a clear-cut explanation. The simulated cloud optical parameters are computed as similarly as possible as in the model radiation scheme and the same overlap assumptions for model clouds are used, to allow a comparison of the radiative schemes. However the distribution of cloud fraction and cloud liquid water are not identical since the computation of OLRSIM uses a spectrally truncated representation of the grid point values used within the forecast model's runs. This is considered in large part responsible for the differences b. and c. (and possibly d.) noted above and is clearly reflected in Fig. 6 and 8 and in the warm OLRSIM bias region seen in Fig.7, which arises mostly from tropical regions over both land and sea, but is, however, a common feature at all latitudes. The different behaviour described under a. (and d.), however, will require further investigation.

5.2 *The 1993 dataset.*

Tables 8 and 9 contain global bias and standard deviations respectively for SMP48 and NCS48 for three days in October 1993. The results for the 1993 data, regarding the differences between OLRSIM and OLRTOV, closely follow those presented for 1989 and will not be discussion again here. Some important differences are noted however, and are discussed in the following paragraphs.

The modifications introduced in cycle 48 do not seem to produce a better fit of the operational model SPM48 to the OLRTOV data, when compared to the SPM46 results. The

NCS48 model however produces a large bias reduction, particularly over sea for NOAA-11 and over land for NOAA-12. Comparing SPM48 to NCS48, the reduction in global bias between OLRSIM and OLRTOV is significant but is not accompanied by a significant reduction in standard deviation. The differences seen over land are again smaller in both bias and standard deviations than those over sea.

The zonal distribution between OLRSIM and OLRTOV for experiment NCS48 is shown in Table 10. The bias reduction going from SPM48 (not shown) to NCS48 is apparent at all latitude bands except over sea in both polar regions, as discussed for the 89 dataset.

Again a large zonal variability of bias and standard deviation is evident but maximum values of standard deviation are now found in the equatorial region where an ITCZ less developed than in February 1989 is now located. A relatively large warm bias is observed across the Equator. Figs. 9a and 9b are the cross sections for the whole data set for experiments SPM48 and NCS48. The two distributions possess many of the features already noted for the 1989 dataset except that a warm bias is now apparent in the longwave fluxes emerging from desert lands in clear sky conditions. Since the ECT for the two satellites differs by about 3 hours and 20 minutes, against the almost six hours in 1989, we do not have data for the warmest hours of the day and it is very difficult to identify a phase error in surface skin temperature as was possible for 1989. It is quite clear however that the new surface physics introduced in cycle 48 is producing window channel (HIRS/2 channel8) brightness temperatures that are too high by 5 to 8 degrees during the daylight hours with a corresponding OLR differences of up to 35 Wm^{-2}, and too cold by up to 5 degrees at night (OLR difference of up to 20 Wm^{-2}).

Table 11 contains the zonal statistics for OLRMOD versus OLRTOV and Table 12 the same for OLRMOD versus OLRSIM. There is not much to add to the discussion of the corresponding 1989 dataset, results shown in Tables 6 and 7.

6. Conclusions.

About six days of HIRS/2 and MSU data have been processed with the aim of understanding to what extent simulated raw radiances produced by the forecast model, initialized with the operational analysis, match the measured values. This exercise is a necessary first step toward using raw radiances to derive cloud parameters, together with the atmospheric temperature and humidity profiles.

Radiance simulations are based on model fields obtained from a short-range (24 to 48 hours) forecast so that spin-up effects are mostly avoided and the description of the dynamical fields is still accurate. The simulations involve cloud parameters, cloud fraction and cloud liquid water. For the present exercise the radiative properties of clouds are computed as similarly as possible to the operational radiation scheme. Estimates of OLR obtained from the measured

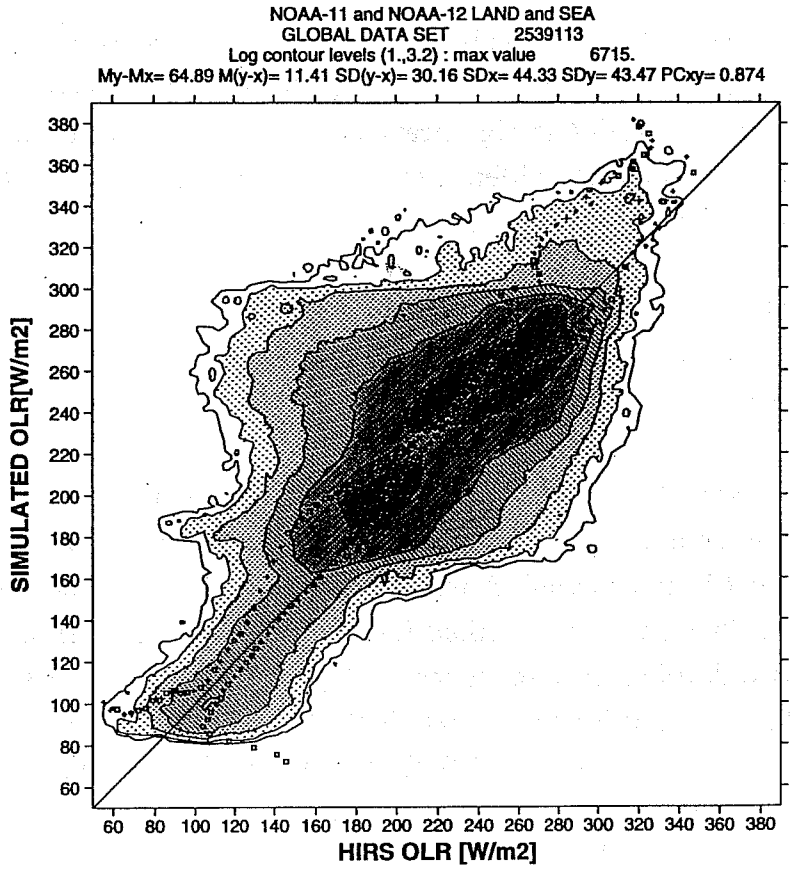

Fig. 9a. Bi-dimensional histogram of OLR computed from measured HIRS/2 radiances (OLRTOV) versus simulated values (OLRSIM) using forecast model SPM48. Period: from 00GMT 14 Oct. 1993 to 06GMT 16 Oct. 1993.

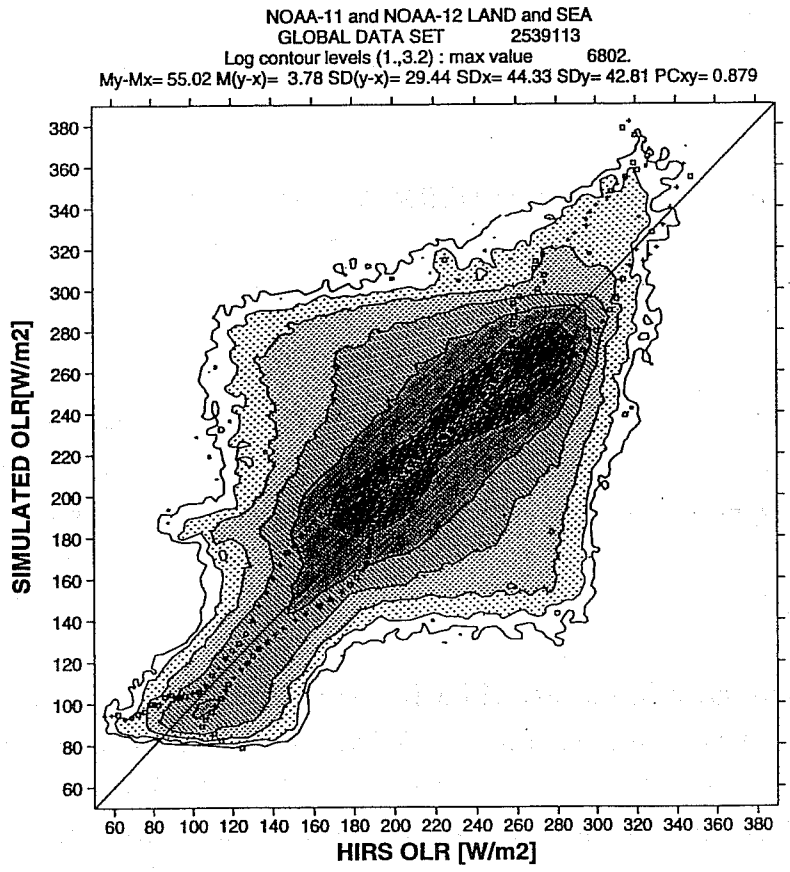

Fig. 9b. As in Fig. 9a. but OLRSIM is computed using forecast model NCS48.

TABLE 10

Zonal bias and standard deviation of the differences between OLRSIM and OLRTOV (Wm^{-2}). Data for NOAA-11 and NOAA-12. Model: NCS48. 1993 dataset.

	OVER LAND			OVER SEA		
LAT	NTOT	BIAS	STDEV	NTOT	BIAS	STDEV
-80.0	167651	-3.4	17.3	56157	20.0	17.1
-60.0	20660	5.0	15.0	282281	8.0	21.5
-40.0	23988	.9	30.4	266418	1.7	27.8
-20.0	80142	2.9	34.3	207681	1.0	20.8
.0	75215	20.2	42.3	211581	6.3	38.8
20.0	94422	-3.2	29.4	193518	3.9	38.3
40.0	148541	-6.4	26.4	147157	2.0	28.2
60.0	221336	5.6	19.2	91694	.0	24.8
80.0	77619	1.9	13.8	173052	10.2	15.5

TABLE 11

Zonal bias and standard deviation of the differences between OLRMOD and OLRTOV (Wm^{-2}). Data for NOAA-11 and NOAA-12. Model: NCS48. 1993 dataset.

	OVER LAND			OVER SEA		
LAT	NTOT	BIAS	STDEV	NTOT	BIAS	STDEV
-80.0	167651	6.7	15.0	56157	15.0	19.5
-60.0	20660	7.3	13.9	282281	1.1	22.7
-40.0	23988	3.8	32.4	266418	4.9	30.0
-20.0	80142	11.0	35.2	207681	17.9	27.6
.0	75215	23.2	46.4	211581	12.5	50.7
20.0	94422	15.4	31.1	193518	3.7	47.1
40.0	148541	5.8	25.0	147157	3.7	29.4
60.0	221336	7.1	19.7	91694	-3.1	24.5
80.0	77619	11.9	14.5	173052	10.7	16.7

TABLE 12

Zonal bias and standard deviation of the differences between OLRMOD and OLRSIM (Wm^{-2}). Data for NOAA-11 and NOAA-12. Model: NCS48. 1993 dataset.

	OVER LAND			OVER SEA		
LAT	NTOT	BIAS	STDEV	NTOT	BIAS	STDEV
-80.0	167651	10.1	8.5	56157	-5.0	7.2
-60.0	20660	2.3	10.0	282281	-6.9	10.0
-40.0	23988	2.9	16.9	266418	3.3	13.4
-20.0	80142	8.2	21.1	207681	17.0	18.0
.0	75215	3.2	24.4	211581	6.3	31.9
20.0	94422	18.7	21.8	193518	-.1	28.6
40.0	148541	12.3	17.5	147157	1.6	16.1
60.0	221336	1.4	9.8	91694	-3.1	11.8
80.0	77619	9.9	10.3	173052	.5	7.6

(OLRTOV) and from the simulated radiances (OLRSIM), using the same statistical regression, are compared with each other and with the OLR computed by the forecast model (OLRMOD). The resolution of HIRS/2 measurements is about 40 km and therefore higher than the model resolution, which can be estimated at about 80 km. To reduce the effect of sub-grid scale processes present in the measurements, each orbit radiance field and OLR field has been filtered using a bi-dimensional gaussian filtering function to reduce the resolution to a figure close to that of the model.

A number of forecast experiments were run involving 4 different versions of the forecast model: the operational spectral model (SPM) cycle 46 and cycle 48, and the New Cloud Scheme (NCS) updates applied to both the SPM cycles.

The bias between OLRTOV and OLRSIM, computed using the NCS models, is much reduced with respect to the results of the SPMs, while the magnitude of the standard deviation increases. As a possible explanation it has been argued that an improved cloud parametrization in NCS produces more variability in the OLR field which increases the magnitude of the standard deviation in presence of similar displacement errors.

A large underestimation of the OLR field is observed in early afternoon over deserts in clear sky conditions in both the SPM46 and NCS46 models. A phase error in the temporal variation of OLR over land is also observed in the latter models. The improved surface scheme, introduced in SPM48 and NCS48, instead produces a fairly substantial overestimation of OLR fluxes in the same areas during the day and an underestimation of OLR during the night. Examination of simulated and measured brightness temperatures in the window channel 8 of HIRS/2 indicates that the observed biases are essentially due to the parametrization of surface radiative properties.

A large warm bias between OLRSIM and OLRTOV is observed in both polar regions over sea in both datasets. Examination of brightness temperatures in HIRS/2 channel 8 indicates that the likely cause for the bias is too high model surface temperatures over ice.

Overall the data clearly indicate that while SPM model provides a fair description of the geographical extent of the organized convection, it severely underestimates its depth, the OLR derived from measurements being much colder than simulations; differences of 60-100Wm^{-2} are found in any deep convection area over the oceans and over land both in the tropical region and at mid-latitudes. The NCS models shows a very different OLR distribution. The description of mid latitude systems is improved. Much lower values of OLR are found in convective areas, denoting a more vigorous cloud development, but they cover only a fraction of the real convective regions.

The comparison between OLRMOD and OLRSIM shows differences even with the data from

the best performing of the models, the NCS48. In the latitude band from 30N to 30S in cloudfree areas OLRMOD is clearly higher than OLRSIM (and OLRTOV) by up to 30 Wm^{-2}; convective areas as described by OLRMOD are clearly more widespread and at mid latitudes, up to 65N ans 65S, OLRMOD frontal regions are colder and their spatial extent is larger than as seen in OLRSIM. Although the simulated cloud optical parameters are computed as in the model radiation scheme and the same overlap assumptions for model layer clouds are being used, the radiative modelling of OLR is very different and the distribution of cloud fraction and cloud liquid water is somewhat different, as discussed in the text. Until the latter problem is solved there is no way to obtain a clear cut explanation of the observed differences.

These results are not to be considered exhaustive as the present work can best be described as work in progress. The same analysis methods can be applied to specific areas to verify the ability of the model in different surface and atmospheric (including cloud) conditions. Moreover the information contained in the set of HIRS/2 and MSU radiances has not yet been fully exploited. It already shows however the potential of comparing the raw measurements of a specific instrumental set, in the present case the TOVS sounding system, to simulations based on all the pertinent model fields.

7. References

Amato U., V. Cuomo, G. Pavese, R. Rizzi, C. Serio and V. Tramutoli, Cloud clearing with radial basis functions. Technical Proceedings of the Sixth International TOVS Study Conference, May 1-6 1991, available from CIMSS Wisconsin.

Beljaars A.C.M. and A.K. Betts, Validation of the boundary layer representation in the ECMWF model. Proceedings of the ECMWF Seminar on Validation of Models over Europe, 7-11 September 1992, pp. 159-196, ECMWF, Reading.

Betts A.K., J.H. Ball and A.C.M. Beljaars, Comparison between the land surface response of the European Centre Model and the FIFE-1987 data. Submitted to Quart. J. Roy. Meteor. Soc. (1993)

Browning K A, Survey of perceived priority issues in the parametrization of cloud-related processes in GCMs. Q.J.R.Meteorol.Soc., 120, 483-487 (1994).

Ellingson R.G., D.J. Yanuk, Hai-Tien Lee and A. Gruber, A technique for estimating outgoing longwave radiation from HIRS radiance observations, J. Of Atmos. Ocean. Techn. 6,706-711, 1989.

Ellingson R.G., Hai-Tien Lee and A. Gruber, Validation of a technique for estimating outgoing longwave radiation from HIRS radiance observations, Seventh American Meteorological Society Conference on Atmospheric Radiation, July 23-27 1990, San

Francisco, California.

Eyre J R, A fast radiative transfer model for satellite sounding systems. ECMWF Research Department Technical Memorandum No. 176, March 1991.

Eyre J R, G A Kelly, A P McNally, E Andersson and A Persson, Assimilation of TOVS radiance information through one-dimensional variational analysis. Q.J.R.Meteorol.Soc. 119, 1427-1463 (1993).

Hamill T M, R P d'Entremont and J T Bunting, A description of the Air Force real time nephanalysis model. Wea. Forecasting, 7, 288-306, 1992.

Heymsfield A.J. and L.J. Donner, A scheme for parametrizing ice-cloud water content in general circulation models, J. Atmos. Sci., 47, 1865-1877, 1990.

Hou Yu-Tai, K A Campana, K E Mitchell,S-K Yang and L L Stowe, Comparison of an experimental NOAA AVHRR cloud dataset with other observed and forecast cloud datasets. J. Atmos. Oceanic Techn. 10,833-849, 1993.

Miller M., A.C.M. Beljaars and T.N. Palmer, The sensitivity of the ECMWF model to the parametrization of evaporation from tropical oceans, J. Clim. 5, 418-434, 1991.

Morcrette J.J., Evaluation of model generated cloudiness: satellite observed and model generated diurnal variability of brightness temperature. Mon. Wea. Rev. 119, 1205-1224, 1991.

Morcrette J.J., Radiation and cloud radiative properties in the ECMWF operational weather forecast model, J. Geo. Res. 96D, 9121-9132, 1991.

Ritter B., Validation of radiation and clouds. Proceedings of ECMWF Seminar on Validation of Models over Europe, 7-11 September 1992, pg 227-264.

Rossow W B and R A Schiffer, ISCCP cloud data products. Bull. Amer. Meteor. Soc., 72, 2-19, 1991.

Slingo J.M., The development and verification of a cloud prediction scheme for the ECMWF model, Q.J.R.Meteor.Soc., 113, 899-927, 1987.

Smith W.L. and H.M. Woolf, Geostationary satellite sounder (VAS) observations of longwave radiation flux, Proc. of the Conference on Satellite Systems to Measure Radiation Budget Parameters and Climate Change Signals, Igls, Austria, 29 August - 2 September, 1983.

Stowe L L, E P McClain, R Carey, P Pellegrino, G Gutman, P Davis, C Long and S Hart, Global distribution of cloud cover derived from NOAA/AVHRR operational satellite data. Adv. Space Res. 11, 51-54, 1991.

Tiedtke M., Representation of clouds in large-scale models, Mon. Wea. Rev., 121, 3040-3061, 1993.